Supplement S1: Technical Description of Plant Hydraulics Module as embedded in TFS

1. Darcy's law treatment of water flux within the continuum

The soil-root-stem-leaf-atmosphere continuum in this model is approximated as a one-dimensional system (see Fig S1.1 below). With the exception of the stem porous medium type, which can take on a variable number of compartments (n_{stem}), the leaf, transporting root, and absorbing root porous medium types are all represented by a single water storage compartment. With reference to Fig. S1.1, according to Darcy's law, the total flux Q_i (kg s^{-1}) in between compartments i and $i+1$, where i indexes water storage compartments from the canopy ($i=0$) to the last rhizosphere element ($i = n_{stem} + n_{shell} + 2$), and flow is positive moving towards the canopy (in the direction of decreasing i), is given by

$$Q_i = -K_i \Delta h_i \tag{S1}$$

where K_i is the total conductance (kg MPa^{-1} s^{-1}) at the boundary of compartments i and $i+1$ and Δh_i is the total water potential difference between the compartments:

$$\Delta h_i = \rho_w g (z_i - z_{i+1}) + (\psi_i - \psi_{i+1}) \tag{S2}$$

where z_i is compartment distance above (+) or below (-) the soil surface (m), ρ_w is the density of water (= 10^3 kg m^{-3}), g is acceleration due to gravity (=9.8 m s^{-2}) and ψ_i is xylem or soil matric water potential (MPa). K_i is treated here as the product of a maximum boundary conductance between compartments i and $i+1$ ($K_{max,i}$), and the fractional loss of conductance of one of the adjacent compartments (FMC_i or FMC_{i+1}), according to:

$$K_i = \begin{Bmatrix} \begin{matrix} K_{max,i} FMC_{i+1} & \Delta h_i < 0 \\ K_{max,i} FMC_i & \Delta h_i \geq 0 \end{matrix} & i \neq n_{stem} + 2 \\ \left[\dfrac{1}{K_{max,aroot,radial} FMC_i} + \dfrac{1}{K_{max,aroot \leftrightarrow r_{node,1}} FMC_{i+1}} \right]^{-1} & i = n_{stem} + 2 \end{Bmatrix} \tag{S3}$$

where $\Delta h_i < 0$ and $\Delta h_{i-1} < 0$ indicate flow *towards* and *away from* the canopy, respectively. This rule is based on the assumption that the conductivity upstream of water flow limits the conductance at the boundary between compartments.

Each $K_{max,i}$ at compartment *boundaries* in this model scales from maximum conductivity ($k_{max,i}$; kg MPa^{-1} m^{-1} s^{-1}) at compartment *nodes* by accounting for the geometry of the flow path either in plant xylem or rhizosphere soil, as discussed in the next section. The exception for the boundary conductance in between the absorbing root and innermost rhizosphere compartments (at $i = n_{stem} + 2$) is because separate maximum conductances are specified internal to the absorbing root ($K_{max,aroot,radial}$) and from the innermost rhizosphere compartment to the absorbing root surface ($K_{max,aroot \leftrightarrow r_{node,1}}$) (see Fig S1.1 and Eqns S19, S24 below).

Figure S1.1: Structure of hydrodynamic portion of plant hydraulics model. Dashed lines indicate compartment boundaries and dots indicate compartment nodes. Plant hydraulics variables are defined either at compartment nodes, boundaries, or cumulatively across a range of compartment nodes. Symbols are defined in this Supplement S1.

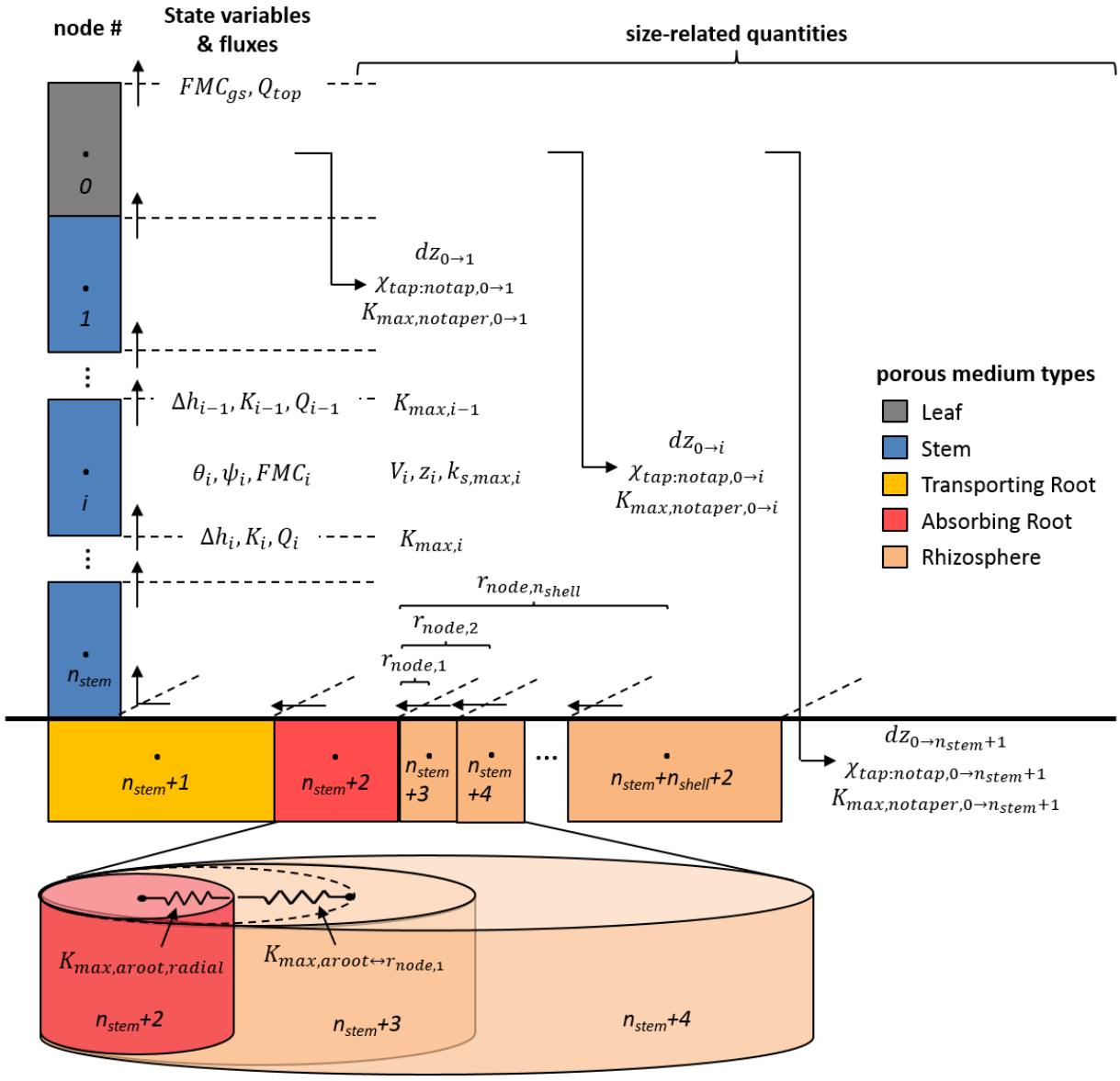

2. Scaling conductivity to conductance throughout the continuum

2.1 Trees

2.1.1 Trees aboveground

There is a near-universal tendency for the radius of xylem conduits to taper with height within a tree (see Section 2.1.4 in main text). Considered in the opposite direction, conduits widen from branch tips to stem base. According to the Hagen-Poiseuille equation, the theoretical maximum total conductance (kg MPa^{-1} s^{-1}) of a xylem conduit is inversely proportional to conduit length and directly proportional to conduit radius as

$$K_{max,theo} = \frac{Q}{\Delta\psi} = \frac{\rho_w \pi r^4}{8\mu L} \quad \text{(S4a)}$$

where Q is the total flux rate (kg s^{-1}), $\Delta\psi$ is the water potential difference at tube ends (MPa), r is the conduit radius (m), μ is the dynamic viscosity (MPa s), and L is the tube length (m). Normalizing for conduit length and cross-sectional area (A; m^2), Eqn S4a in terms of maximum conductivity (kg m^{-1} MPa^{-1} s^{-1}) is

$$k_{max,theo} = \frac{QL}{\Delta\psi A} = \frac{\rho_w r^2}{8\mu} \quad \text{(S4b)}$$

Because conduit radius increases from tree top to tree base, $k_{max,theo}$ also increases. Assuming that actual maximum xylem-specific hydraulic conductivity ($k_{s,max,x}$) varies in proportion to theoretical conductivity ($k_{s,max,x} \propto k_{max,theo} \propto r^2$), it therefore follows that a positive benefit (increase) on total integrated plant conductance results from the widening of xylem conduits from tree top to base.

Savage et al. (2010) considered this effect by modeling theoretical trees in which terminal branch (petiole) properties (branch and conduit radii and lengths) were invariant across trees of different sizes, but which increased towards tree base according to rules assuming fractal, self-similar branching and space-filling geometry in an external (tree branches) and internal (xylem conduits) branching network. Such rules allowed them use the Hagen-Poiseuille equation to sum hydraulic resistivities occurring in series and conductivities in parallel in order to predict whole-tree aboveground conductance with and without accounting for conduit taper. Because we used the Savage et al. (2010) result to account for the effects of xylem taper on whole plant conductance in our model, and because their results are referenced to the invariant terminal petiole properties, we needed to first standardize $k_{s,max,x}$, which is measured on non-terminal branches, to a corresponding value in the petiole. By assuming that $k_{s,max,x} \propto k_{max,theo} \propto r^2$, we estimated the ratio of $k_{max,x}$ in petioles ($k_{s,max,petiole}$) to that at a reference point ($k_{s,max,ref}$) as

$$\frac{k_{s,max,petiole}}{k_{s,max,ref}} = \frac{\rho_w r_{int,petiole}^2 \Big/ 8\mu}{\rho_w r_{int,ref}^2 \Big/ 8\mu} = \left(\frac{r_{int,petiole}}{r_{int,ref}}\right)^2 \quad \text{(S5)}$$

which, when rearranged, gives Step 1 of our 3-step process for accounting for xylem taper (see Section 2.1.4 of main text):

$$k_{s,max,petiole} = k_{s,max,ref}\left(\frac{r_{int,petiole}}{r_{int,ref}}\right)^2 \quad \text{(S6)}$$

where $r_{int,ref}$ and $k_{s,max,ref}$ are the reference mean conduit radius and reference $k_{s,max,x}$ characteristic of branches where was measured and $r_{int,petiole}$ is the radius of conduits in petioles. $r_{int,petiole}$ is given by the corresponding value used in the Savage et al. (2010) model (10 μm), and $r_{int,ref}$ is given by one half the mean value hydraulically-weighted conduit diameter (d_h = 22 μm) as measured for all tropical angiosperm trees within the XFT database.

Assuming $k_{s,max,x} = k_{s,max,petiole}$ everywhere, we can estimate whole-tree aboveground conductance in the absence of xylem taper (Step 2; see Section 2.1.4 of main text) as

$$K_{max,tree,notaper,ag} = \frac{k_{s,max,petiole}A_l}{\Delta z A_l : A_s} = \frac{k_{s,max,petiole}A_s}{\Delta h} \quad \text{(S7)}$$

where Δz (m) is the height difference from canopy top to the depth of the transporting root just below the ground surface, $A_l : A_s$ is the leaf to sapwood area ratio (m^2 cm^{-2}) and A_l (m^2) is the total tree leaf area, respectively.

Finally, to estimate whole-tree aboveground conductance accounting for xylem taper ($K_{max,tree,ag}$), we must multiply $K_{max,tree,notaper,ag}$ by a nondimensional factor representing the ratio of theoretical whole-tree aboveground conductance with taper to that without ($\chi_{tap:notap,ag}$) (Step 3 of Section 2.1.4 of main text):

$$K_{max,tree,ag} = K_{max,tree,notaper,ag}\chi_{tap:notap,ag} \quad \text{(S8)}$$

where $\chi_{tap:notap,ag}$ is derived from the Savage et al. (2010) model below. This model has an external branching network that is space-filling and an internal xylem conduit network that maximizes hydraulic conductance while protecting against embolism. A key component of this model is the incorporation of tapering of xylem conduits from one branching level to the next, expressed as the ratio of daughter branch (k) to parent branch ($k+1$) xylem conduit radii ($r_{int,k}/r_{int,k+1} = {n_{ext}}^{-p/2}$). The number of daughter branches per parent branch (n_{ext}) takes a constant value of 2 in this model, and $r_{int,k}/r_{int,k+1}$ is less than one (xylem taper) when the xylem taper exponent p is greater than zero. In particular, the degree of xylem taper is optimal (in terms of maximizing whole-tree hydraulic conductance while protecting against embolism) when $p = 1/3$, which, unless otherwise indicated, is the value used in all of the simulations in this paper. Observations suggest that p is bounded on [1/6, 1/3] (Savage et al. 2010). A taper exponent of 1/3 amounts to $\chi_{tap:notap}$ in the range of 23-50 for trees of heights 10-30 m; thus the benefit of xylem taper for increasing total plant conductance itself increases with tree height.

With reference to compartment indexing shown in Fig. S1.1, $\chi_{tap:notap,0\to i}$ is defined as the ratio of integrated conductance with taper ($p > 0$ in the Savage et al. (2010) model) over some tree height interval from petiole (i = 0) to the ith plant compartment ($K_{max,p>0,0\to i}$) to that without ($K_{max,p=0,0\to i}$, or synonymously, $K_{max,notaper,0\to i}$):

$$\chi_{tap:notap,0\to i} \equiv \frac{K_{max,p>0,0\to i}}{K_{max,p=0,0\to i}} \tag{S9}$$

Because trees in the Savage et al. (2010) model are self-similar, the sub-tree represented by the height interval spanning $0 \to i$ ($H_{0\to i}$) is equivalent to a single entire tree of height $H = H_{0\to i}$, thus allowing the total conductance over this height interval to be equated to the Savage et al. (2010) model prediction of total integrated aboveground (subscript ag) conductance $K_{max,p,tree,ag}$ (units kg s^{-1} Pa^{-1} in their model):

$$K_{max,p,0\to i} = K_{max,p,tree,ag}(H_{0\to i}) \tag{S10}$$

where the subscript p indexes a particular taper exponent value. Fig. 2a of Savage et al. (2010) gives $K_{max,p,tree,ag}$ as a function of the ratio of petiole to basal tree branch outer radii ($r_{ext,petiole}$ and $r_{ext,base}$, respectively) as:

$$K_{max,tree,ag,p} = a_p \left(\frac{r_{ext,base}}{r_{ext,petiole}}\right)^{b_p} \tag{S11}$$

where a_p and b_p are normalizing constants which we obtained from their Fig 2a (a_p = 7.20E-13, 6.58E-13, 6.67E-13 kg s^{-1} Pa^{-1} and b_p = 1.32, 1.63, 1.85 for p = 0, 1/6, and 1/3, respectively). The radii ratio is also expressed in terms of n_{ext}, the number of daughter branches per parent branch (= 2 in their model), and N, the total number of branching levels, as

$$\frac{r_{ext,base}}{r_{ext,petiole}} = n_{ext}^{N/2} \tag{S12}$$

N relates to tree height (H; m) in their model via

$$N = \frac{3\ln(1 - \frac{H}{L_{petiole}}(1 - n_{ext}^{1/3}))}{\ln n_{ext}} - 1 \tag{S13}$$

where $L_{petiole}$ is petiole length (= 0.04 m in their model). Combining equations S9-S13 allows us to estimate $\chi_{tap:notap,0\to i}$ as a function of the height difference between any two compartments ($H_{0\to i}$).

So far we have derived how to obtain whole tree maximum hydraulic conductance with and without taper. To obtain the component maximum hydraulic conductances between any two

adjacent compartments *i* and *i*+1 ($K_{max,i}$), we must difference the integrated hydraulic resistances adjacent to a boundary of interest as

$$K_{max,i} = \begin{cases} K_{max,notaper,0\to i+1} \cdot \chi_{tap:notap,0\to i+1} & i = 0 \\ \left[\frac{1}{K_{max,notaper,0\to i+1} \cdot \chi_{tap:notap,0\to i+1}} - \frac{1}{K_{max,notaper,0\to i} \cdot \chi_{tap:notap,0\to i}}\right]^{-1} & 0 < i \le n_{stem} \end{cases} \quad \text{(S14)}$$

$K_{max,notaper,0\to i+1}$ is estimated using Eqn S7. Applying Eqn S14 over $0 < i \le n_{stem}$ allows the effects of taper to be extended slightly belowground to include the maximum conductance at the boundary between the bottom-most stem compartment ($i = n_{stem}$) and the transporting root compartment ($i = n_{stem} + 1$).

2.1.2 Trees belowground

Note: In this section, minimum resistance refers to the inverse of maximum conductance. We defined a quantity, $R_{frac,stem}$, as the fraction of total tree minimum resistance (represented by total aboveground resistance ($R_{min,tree,ag}$). We used a study which quantified total aboveground and belowground resistance in tropical trees (Fisher et al., 2006) under near-saturated (wet season) conditions to specify $R_{frac,stem} = 0.625$ and then estimated the total tree minimum resistance and belowground minimum resistance accordingly. In terms of equations,

$$K_{max,tree,ag} = \left(\sum_{i=0}^{n_{stem}} \frac{1}{K_{max,i}}\right)^{-1} = K_{max,notaper,0\to n_{stem}+1} \cdot \chi_{tap:notap,0\to n_{stem}+1} \quad \text{(S15)}$$

$$\frac{1}{K_{max,tree,ag}} = R_{min,tree,ag} = R_{frac,stem} R_{min,tree,tot} \quad \text{(S16)}$$

Rearranging S16 gives

$$K_{max,tree,tot} = R_{frac,stem} K_{max,tree,ag} \quad \text{(S17)}$$

The total belowground maximum tree conductance is therefore

$$K_{max,tree,bg} = \left[\frac{1}{K_{max,tree,tot}} - \frac{1}{K_{max,tree,ag}}\right]^{-1} \quad \text{(S18)}$$

Finally, we equally partitioned the total belowground minimum tree resistance among the transporting root-absorbing root ($K_{max,n_{stem}+1}$) and absorbing root node-to-root surface ($K_{max,aroot,radial}$) pathways, which represent, respectively, axial (in xylem) and radial (combined apoplastic and symplastic pathways of root water uptake) resistances.

$$K_{max,n_{stem}+1} = K_{max,aroot,radial} = 2 * K_{max,tree,bg} \quad \text{(S19)}$$

See Fig S1.1 for the diagrammatic representation of these two components.

2.2 Rhizosphere

As in Gardner (1960) and the Sperry et al. (1998) model (hereafter S98), we represented absorbing roots as vertically oriented line sinks assumed to be well-mixed (regardless of the individual tree to which they belong) over a defined total soil volume, which allows the mean distance between roots, and thus the characteristic radius of an individual root's rhizosphere ($r_{out,n_{shell}}$), to be constant across individual absorbing roots and be represented as a function of total community root length ($l_{aroot,comm} = \sum_{j=1}^{j=n_{trees}} l_{aroot,i}$; m) as

$$r_{out,n_{shell}} = \left(\frac{2\pi l_{aroot,comm}}{A_{plot} Z_{soil}}\right)^{-0.5} \quad \text{(S20)}$$

Where r_{out} (m) denotes the outer radius of each concentric rhizosphere compartment cylinder (a "shell"), n_{shell} is a specified number of rhizosphere shells, A_{plot} is the plot area (m^2) and Z_{soil} is soil depth (m). Rhizosphere shells are concentrated near the absorbing root where water potential gradients are largest, following

$$r_{out,k} = r_{aroot}\left(\frac{r_{out,n_{shell}}}{r_{aroot}}\right)^{\frac{k}{n_{shell}}} \quad \text{(S21)}$$

Where *k* indexes a soil compartment [1, n_{shell}] according to Fig S1.1 and r_{aroot} is absorbing root radius. The radius at the node (midpoint) of a rhizosphere shell is

$$r_{node,k} = \begin{cases} 0.5(r_{aroot} + r_{out,k}) & k = 1 \\ 0.5(r_{out,k-1} + r_{out,k}) & 1 < k \leq n_{shell} \end{cases} \quad \text{(S22)}$$

The maximum boundary conductances between adjacent rhizosphere shells (boundary values indexed by *k* for shells *k* and *k*+1) is given by

$$K_{max,k} = \frac{\pi l_{aroot,comm}}{\ln\left(r_{node,k+1}/r_{node,k}\right)} k_{max,soil} \quad 1 \leq k \leq n_{shell} - 1 \quad \text{(S23)}$$

where $k_{max,soil}$ is the saturated soil hydraulic conductivity (kg m^{-1} s^{-1} MPa^{-1}). At the outermost rhizosphere shell $r_{out,n_{shell}}$, by model construction there is a zero net flux and hence a zero boundary condition, which is why $K_{max,n_{shell}}$ remains undefined. The conductance in between the innermost rhizosphere shell node and the absorbing root surface (see Fig S1.1) is

$$K_{max,aroot \leftrightarrow r_{node,1}} = \frac{\pi l_{aroot,j}}{\ln\left(r_{node,1}/r_{aroot}\right)} \quad \text{(S24)}$$

The rhizosphere shell boundary conductances ($K_{max,k}$) are then mapped to each tree's (indexed by *j*) one-dimensional plant hydraulics array (indexed by *i*) as

$$K_{max,aroot\leftrightarrow r_{node,1},j} = K_{max,aroot\leftrightarrow r_{node,1}} \frac{l_{aroot,j}}{l_{aroot,comm}} \quad \text{(S25a)}$$

$$K_{max,i=(n_{stem+2}+k),j} = K_{max,k,j} \frac{l_{aroot,j}}{l_{aroot,comm}} \quad 1 \le k \le n_{shell} \quad \text{(S25b)}$$

The total maximum conductance in between the absorbing root node and innermost rhizosphere shell ($K_{max,i=n_{stem+2},j}$), is not explicitly defined because of how K_i is specified here (see Eqn S3).

As of yet there are no tropics-specific pedotransfer functions for estimating saturated soil hydraulic conductivity, $k_{max,soil}$ (kg m^{-1} s^{-1} MPa^{-1}). We used instead the temperate soil pedotransfer function of Cosby et al. (1984):

$$k_{max,soil} = \frac{0.0254 \cdot 10^6}{9.8 * 3600} 10^{-0.60+0.0126(\%sand)-0.0064(\%clay)} \quad \text{(S26)}$$

3. Constitutive equations

3.1 Water potential as a function of water content

This relationship describes the relative ease with which water can be extracted from a porous medium as a function of the quantity of water in that medium. Below we describe this relationship for plant tissue and soil porous medium types. For plants this relationship is commonly described by plant physiologists as a "pressure-volume", or PV, curve (Tyree and Hammel, 1972). For soil, this is commonly described by soil physicists as a "soil water characteristic," or SWC, curve. Common to both relationships are parameters describing the saturated and residual water contents (θ_{sat}).

3.1.1 PV curves in trees

Equations 1-3 in the main text of this article give PV curves in terms of relative water content (RWC; g H_2O g^{-1} H_2O at saturation). Below we give them in terms of volumetric water content (θ; m^3 H_2O m^{-3} plant tissue), by using the transformation

$$RWC = \frac{W}{\rho_w \theta_{sat}} = \frac{\rho_w \theta}{\rho_w \theta_{sat}} = \frac{\theta}{\theta_{sat}} \quad \text{(S27)}$$

Where W is water mass (g) and θ_{sat} (m^3 m^{-3}) is the maximum water content on a per unit tissue volume basis (or porosity). This gives, respectively, for equations 1-3 in the main text, where *i* indexes water storage compartments as given in Fig. S1.1:

$$\psi_i(\theta_i) = \begin{cases} \psi_0 - m_{cap}\left(\frac{\theta_{sat}-\theta_i}{\theta_{sat}}\right) & \theta_{sat} RWC_{ft,i} \le \theta_i \le \theta_{sat,i} \\ \psi_{sol,i}(\theta_i) + \psi_{p,i}(\theta_i) & \theta_{sat} RWC_{tlp,i} \le \theta_i < \theta_{sat,i} RWC_{ft,i} \\ \psi_{sol,i}(\theta_i) & \theta_{sat} RWC_{r,i} \le \theta_i < \theta_{sat,i} RWC_{tlp,i} \end{cases} \quad 0 \le i \le n_{stem} + 2 \quad \text{(S28)}$$

$$\psi_{sol,i}(\theta_i) = \frac{-|\pi_{o,i}|\theta_{sat,i}(RWC_{ft,i} - RWC_{r,i})}{(\theta_i - \theta_{sat,i}RWC_{r,i})} \quad \text{(S29)}$$

$$\psi_{p,i}(\theta_i) = |\pi_{o,i}| + \varepsilon_i \frac{(\theta_i - \theta_{sat,i}RWC_{ft,i})}{\theta_{sat,i}(RWC_{ft,i} - RWC_{r,i})} \quad \text{(S30)}$$

Tissue porosities are estimated either using knowledge about tissue saturated mass (leaves) or cell wall density (all other tissues).

$$\theta_{sat,i} = \begin{cases} \frac{\rho_{leaf}}{\rho_w}\left(\frac{1}{dfw} - 1\right) & 0 \le i < 1 \\ WD/\rho_c & 1 \le i \le n_{stem} + 2 \end{cases} \quad \text{(S31)}$$

where for leaves *dfw* is the dry:fresh mass ratio and is empirically determined as a function of specific leaf area (SLA) following Stewart et al. (1990):

$$dfw = -0.21 * \log SLA \; + \; 1.431 = -0.21 * \log \frac{1E4}{LMA} \; + \; 1.431 \quad \text{(S32)}$$

and xylem porosity is assumed constant across stem, transporting root and fine root tissues and is determined assuming a constant cell wall density ρ_c = 1.54 g cm^{-3} (Siau, 1984).

As shown in the main text, the three equations of S28 comprise three successive regions, respectively: a capillary drainage region ($capillaryPV(\theta)$), followed by an elastic drainage region ($elasticPV(\theta)$), and then a final embolism region ($embolismPV(\theta)$). In practice, we do not strictly apply the plant PV curve in a three-phase piecewise manner as Eqn S28 implies; instead we applied a two-phase quadratic smoothing to Eqn S28 to ensure that the function had no discontinuities, where *i* indexes water storage compartments as given in Fig. S1.1:

$$\psi_i(\theta_i) = T(\theta_i) \quad 0 \le i \le n_{stem} + 2 \quad \text{(S33a)}$$

where the right hand side of Eqn S33a derives from

$$c(\theta_i) = elasticPV(\theta_i) * capillaryPV(\theta_i) \quad \text{(S33b)}$$

$$b(\theta_i) = -1 * [elasticPV(\theta_i) + capillaryPV(\theta_i)] \quad \text{(S33c)}$$

$$t(\theta) = \frac{-b(\theta_i) - \sqrt{b(\theta_i)^2 - 4\beta_1 c(\theta_i)}}{2\beta_1} \quad \text{(S33d)}$$

$$C(\theta_i) = t(\theta_i) * embolismPV(\theta_i) \quad \text{(S33e)}$$

$$B(\theta_i) = -1 * [t(\theta_i) + embolismPV(\theta_i)] \quad \text{(S33f)}$$

$$T(\theta_i) = \frac{-B(\theta_i) + \sqrt{B(\theta_i)^2 - 4\beta_2 C(\theta_i)}}{2\beta_2} \quad \text{(S33g)}$$

A minus (-) sign is used in front of the radical in S33d because the function is concave down at this junction, and a plus (+) sign is used in front of the radical in S33g because the joint function is concave up at this junction. We chose values of β_1=0.8 and β_2=0.99. These functions are also continuously differentiable (needed for numerical solution), giving

$$\frac{d\psi_i(\theta_i)}{d\theta_i} = \frac{dT(\theta_i)}{d\theta_i} \quad 0 \le i \le n_{stem} + 2 \quad \text{(S34a)}$$

where the right-hand side of S34a derives from

$$\frac{d\big(capillaryPV(\theta_i)\big)}{d\theta_i} = \frac{m_{cap}}{\theta_{sat}} \quad \text{(S34b)}$$

$$\frac{d(elasticPV(\theta_i))}{d\theta_i} = \frac{d\psi_{sol,i}(\theta_i)}{d\theta_i} + \frac{d\psi_{p,i}(\theta_i)}{d\theta_i} \quad \text{(S34c)}$$

$$\frac{d\big(embolismPV(\theta_i)\big)}{d\theta_i} = \frac{d\big(\psi_{sol}(\theta_i)\big)}{d\theta_i} \quad \text{(S34d)}$$

$$\frac{d\psi_{sol,i}(\theta_i)}{d\theta} = \frac{\left|\pi_{o,i}\right|\theta_{sat,i}(RWC_{ft,i} - RWC_{r,i})}{(\theta_i - \theta_{sat,i}RWC_{r,i})^2} \quad \text{(S34e)}$$

$$\frac{d\psi_{p,i}(\theta_i)}{d\theta} = \frac{\varepsilon_i\theta_i}{\theta_{sat,i}(RWC_{ft,i} - RWC_{r,i})} \quad \text{(S34f)}$$

$$\frac{dc(\theta_i)}{d\theta} = elasticPV(\theta_i) * \frac{d\big(capillaryPV(\theta_i)\big)}{d\theta_i} + capillaryPV(\theta_i) * \frac{d(elasticPV(\theta_i))}{d\theta_i} \quad \text{(S34g)}$$

$$\frac{db(\theta_i))}{d\theta_i} = -1 * \left[\frac{d(elasticPV(\theta_i))}{d\theta_i} + \frac{d(capillaryPV(\theta_i))}{d\theta_i}\right] \quad \text{(S34h)}$$

$$\frac{dt(\theta_i)}{d\theta} = \frac{1}{2\beta_1}\left[\frac{-db(\theta_i)}{d\theta_i} - 0.5\left(\left(b(\theta_i)^2 - 4\beta_1 c(\theta_i)\right)^{-0.5}\right)\left(2b(\theta_i)\frac{db(\theta_i)}{d\theta_i} - 4\beta_1\frac{dc(\theta_i)}{d\theta_i}\right)\right] \quad \text{(S34i)}$$

$$\frac{dC(\theta_i)}{d\theta_i} = t(\theta_i) * \frac{d\big(embolismPV(\theta_i)\big)}{d\theta_i} + embolismPV(\theta_i) * \frac{dt(\theta_i)}{d\theta_i} \quad \text{(S34j)}$$

$$\frac{dB(\theta_i)}{d\theta_i} = -1 * \left[\frac{dt(\theta_i)}{d\theta_i} + \frac{d(embolismPV(\theta_i)}{d\theta_i}\right] \quad \text{(S34k)}$$

$$\frac{dT(\theta_i)}{d\theta_i} = \frac{1}{2\beta_2}\left[-\frac{dB(\theta_i)}{d\theta_i} + 0.5\left(\left(B(\theta_i)^2 - 4\beta_2 C(\theta_i)\right)^{-0.5}\right)\left(2B(\theta_i)\frac{dB(\theta_i)}{d\theta_i} - 4\beta_2\frac{dC(\theta_i)}{d\theta_i}\right)\right] \quad \text{(S34l)}$$

3.1.2 SWC curves in rhizosphere

We used the van Genuchten (1980) (hereafter VG) functional form for the SWC in the rhizosphere because datasets are published (Tomasella and Hodnett, 2002; hereafter T&H) giving pantropics-specific pedotransfer functions (PTFs: predictions of soil hydraulic properties from soil texture and other easily measured soil properties) based on the parameters in the VG equation:

$$\psi_i = -\frac{1}{\alpha}\left[\Theta_i{}^{-1/m} - 1\right]^{1/n} \quad n_{stem} + 2 < i \leq n_{stem} + n_{shell} + 2 \quad \text{(S35)}$$

where *i* indexes water storage compartments as given in Fig. S1.1, Θ_i is the saturation fraction $\left[\frac{\theta_i - \theta_r}{\theta_s - \theta_r}\right]$, and θ_r, θ_s, α (MPa^{-1}) and n (-) are soil hydraulic properties representing the residual water content (water content at which $\psi_{soil} \to -\infty$), saturated water content (water content at which $\psi_{soil} \to 0$), the inverse of the air entry pressure and the steepness of the SWC related to the pore size distribution, respectively, with m (-) equal to $1 - 1/n$.

The derivative of S35 with respect to water content (required for numerical solution) is

$$\frac{d\psi_i}{d\theta} = \frac{\left(\Theta_i{}^{-\frac{1}{m}} - 1\right)^{\frac{1}{n}-1} * \Theta_i{}^{-\frac{1}{m}-1}}{mn\alpha(\theta_s - \theta_r)} \quad n_{stem} + 2 < i \leq n_{stem} + n_{shell} + 2 \quad \text{(S36)}$$

where $\Theta_i = \left[\frac{\theta_i - \theta_r}{\theta_s - \theta_r}\right]$ as above.

Use of tropics-specific PTFs is important because, given similar textural properties as temperate soils, they tend to have comparatively lower bulk densities and a higher incidence of macropores, which leads to comparatively higher α and θ_s. Additionally, many tropical soils have a bivariate pore size distribution, with a large proportion of their total pore volume in very small pores, which often leads to high values of (θ_r) compared to their tropical counterparts of similar soil texture.

Rather than using the continuous PTFs of T&H, which required variables other than soil texture that are much less widely available such as organic matter content, pH, and cation exchange capacity, we used their "class" PTFs, which comprise a look-up table based on soil texture alone. We used values from Table 6 of T&H, reproduced in Table S1.1 below.

Table S1.1. Tropics-specific VG soil hydraulic properties, from Table 6 of Tomasella and Hodnett (2002).

Soil texture class (USDA)	α (MPa^{-1})	n (-)	θ_s (m^3 m^{-3})	θ_r (m^3 m^{-3})
Sand	380	2.474	0.41	0.037
Loamy sand	837	1.672	0.438	0.062

Sandy loam	396	1.553	0.461	0.111
Loam	246	1.461	0.521	0.155
Silt loam	191	1.644	0.601	0.223
Silt*	191	1.644	0.601	0.223
Sandy clay loam	644	1.535	0.413	0.149
Clay loam	392	1.437	0.519	0.226
Silty clay loam	298	1.513	0.586	0.267
Silty clay	258	1.466	0.57	0.278
Sandy clay	509	1.396	0.46	0.199
Clay	463	1.514	0.546	0.267

* Unavailable in T&H; approximated with values from the closest adjacent textural class (silt loam).

3.2 Hydraulic conductivity as a function of water potential

In both plant and soil porous media, the rate at which water is transported down a unit gradient of water potential declines as water potential gets more negative. In both media, this results from embolism (formation of air pockets) impeding the flow of water. In plants, this relationship is referred to by plant physiologists as the "percent loss of conductivity" or "xylem vulnerability" curve. Based on how we have implemented it in our model, we refer to it as a "fraction of maximum conductivity" (FMC) curve. In soil, it is commonly referred to as the "unsaturated hydraulic conductivity" relationship.

3.2.1 FMC curves in trees

Equation 4 of the main text gives the FMC relationship for trees. Its derivative with respect to xylem water potential also is required for the numerical solution, where *i* indexes water storage compartments as given in Fig. S1.1:

$$\frac{d(FMC_i(\psi_i))}{d\psi_i} = -\frac{a_i}{P_{50,i}}\left(\frac{\psi_i}{P_{50,i}}\right)^{a_i-1}\left[1+\left(\frac{\psi_i}{P_{50,i}}\right)^{a_i}\right]^{-2} \quad 0 \le i \le n_{stem}+2 \qquad \text{(S37)}$$

3.2.2 Unsaturated hydraulic conductivity curves in rhizosphere

van Genuchten (1980) derived a closed form solution for this relationship using the same parameters as in the SWC curve (Eqn S35):

$$FMC_i = \frac{[1-(\alpha|\psi_i|)^{n-1}[1+(\alpha|\psi_i|)^n]^{-m}]^2}{[1+(\alpha|\psi_i|)^n]^{m/2}} \quad n_{stem}+2 < i \le n_{stem}+n_{shell}+2 \qquad \text{(S38)}$$

where *i* indexes water storage compartments as given in Fig. S1.1. Its derivative with respect to water potential is

$$\frac{d(FMC_i)}{d|\psi_i|} = (-1)\left[f_1\frac{df_2}{d|\psi_i|} + f_2\frac{df_1}{d|\psi_i|}\right] \quad n_{stem}+2 < i \le n_{stem}+n_{shell}+2 \qquad \text{(S39a)}$$

where the (-1) arises due to the fact that S38 is based on the *absolute value* of water potential, and where

$$f_1 = (1 - f_{1a}f_{1b})^2 \tag{S39b}$$

$$f_2 = (1 + (\alpha|\psi_i|)^n)^{-\frac{m}{2}} \tag{S39c}$$

$$\frac{df_1}{d|\psi_i|} = 2[1 - f_{1a}f_{1b}]\left[-f_{1a}\frac{df_{1b}}{d\psi_i} - f_{1b}\frac{df_{1a}}{d\psi_i}\right] \tag{S39d}$$

$$f_{1a} = (\alpha|\psi_i|)^{n-1} \tag{S39e}$$

$$\frac{df_{1a}}{d|\psi_i|} = \alpha(n-1)(\alpha|\psi_i|)^{n-2} \tag{S39f}$$

$$f_{1b} = (1 + (\alpha|\psi_i|)^n)^{-m} \tag{S39g}$$

$$\frac{df_{1b}}{d|\psi_i|} = -mn\alpha(\alpha|\psi_i|)^{n-1}(1 + (\alpha|\psi_i|)^n)^{-m-1} \tag{S39h}$$

$$\frac{df_2}{d|\psi_i|} = -\frac{mn\alpha}{2}(\alpha|\psi_i|)^{n-1}(1 + (\alpha|\psi_i|)^n)^{-\frac{m}{2}-1} \tag{S39i}$$

3.3 Stomatal conductance as a function of water potential (FMC_{gs})

Eqn 5 of the main text gives the functional form for the stomatal vulnerability curve, or 'fraction of maximum conductance' for stomata (FMC_{gs}). Its derivative with respect to leaf water potential (ψ_0) (required for numerical solution) is given by

$$\frac{d(FMC_{gs}(\psi_0))}{d\psi_0} = -\frac{a_{gs}}{P_{50,gs}}\left(\frac{\psi_0}{P_{50,gs}}\right)^{a_{gs}-1}\left[1 + \left(\frac{\psi_0}{P_{50,gs}}\right)^{a_{gs}}\right]^{-2} \tag{S40}$$

4. Linking plant hydraulics compartment geometry to TFS tree allometry

4.1 Trees

4.1.1 Compartment heights

With reference to Fig S1.1, the heights (z_i; positive above ground surface and negative below) of the different compartments of the 1D continuum are as follows:

$$z_i = \begin{cases} H & i = 0 \\ (n_{stem} - i + 0.5)dz_{stem} & 0 < i \leq n_{stem} \\ -D(Y = 0.5) & n_{stem} < i \leq n_{stem} + 2 \end{cases} \tag{S41}$$

where H is tree height, n_{stem} is the number of stem compartments (>= 1),

$$dz_{stem} = \frac{H}{n_{stem}} \quad \text{(S42)}$$

and $D(Y = 0.5)$ gives the depth (m) at which 50% cumulative roots are attained, as given by the inverse (obtained using a bisection routine) of the cumulative root distribution function (Y) of Zeng (2001) with parameters a = 7 and b = 1 for broadleaf evergreen trees.

4.1.2 Compartment sizes

With the exception of the stem and fine roots, the volumes of the hydraulic compartments derive from the corresponding TFS biomass pools (kg) and the corresponding density (m^3) of each tissue as follows:

$$V_i = \begin{cases} B_{leaf}/\rho_{leaf} & i = 0 \\ A_s H/n_{stem} & 0 < i \leq n_{stem} \\ B_{coarse}/\rho_{stem} & i = n_{stem} + 1 \\ SA_{fine} r_{fine}/2 & i = n_{stem} + 2 \end{cases} \quad \text{(S43)}$$

4.1.2.1 Foliage

We used the aboveground biomass allometry of Yamakura et al. (1986), which was independent of individual functional traits:

$$B_{leaf} = 0.09146(B_{trunk} + B_{branch})^{0.7266} \quad \text{(S44)}$$

where B_{trunk} and B_{branch} are the biomass of the main stem and branches, respectively (kg), and are given by

$$B_{trunk} = 0.02903(DBH^2 H)^{0.9813} \quad \text{(S45)}$$

$$B_{branch} = 0.1192 B_{trunk}{}^{1.059} \quad \text{(S46)}$$

and where DBH and H are tree diameter at breast height (cm) and height (m), respectively. Leaf tissue density (ρ_{leaf}) is estimated using an empirical relation with LMA (B. Christoffersen and L. Rowland, unpublished data; $R^2 = 0.29$) for a sample of leaves (n=191 leaves over n=8 spp) at the Caxiuana forest site which had paired measurements of leaf dry mass and leaf fresh volume, the latter obtained by multiplying leaf area by leaf lamina thickness obtained using a precision caliper (n=4 per leaf) as

$$\rho_{leaf} = -2.32 \cdot SLA + 782 = -2.32 \cdot 10^4/LMA + 782 \quad \text{(S47)}$$

4.1.2.2 Sapwood

The hydraulically active volume in the stem is derived from sapwood and not the stem biomass because heartwood does not store appreciable quantities of water. Sapwood area (A_s; m^2) was calculated using the leaf:sapwood area ratio:

$$A_s = \frac{A_l}{A_l{:}A_s} 10^{-4} \quad \text{(S48)}$$

where total leaf area (A_l; m^2) is independent of functional traits as given by the Yamakura et al. (1986) allometry:

$$A_l = 11.67 {B_l}^{0.9412} \quad \text{(S49)}$$

In Eqn S43 we assumed that the fraction of stem volume which is sapwood and heartwood remains constant across tree branching levels, and that branching is area-preserving (Savage et al. 2010). This total stem volume is then partitioned equally among the user-specified number of stem compartments (n_{stem}).

4.1.2.3 Coarse roots

The coarse root biomass derives from the difference between total root biomass and fine root biomass:

$$B_{coarse} = B_{root} - B_{fine} \quad \text{(S50)}$$

Coarse root tissue density is assumed to be the same as stem density:

$$\rho_{coarse} = \rho_{stem} = WD * 10^3 \quad \text{(S51)}$$

Total root biomass follows that of Niklas (2005):

$$B_{root} = 0.304 {B_{agr}}^{0.941} \quad \text{(S52)}$$

where $B_{agr} = B_{leaf} + B_{branch} + B_{trunk}$ is total aboveground biomass.

4.1.2.4 Fine (absorbing) roots

Fine root biomass is governed by a user-specified absorbing root area-to-leaf area parameter ($A_l{:}A_r$; $m^2\ m^{-2}$), a constant specific root length ($SRL = 15000$ m kg^{-1} dry mass; derived from Metcalfe et al. (2007)) and an assumed mean value for absorbing root radius ($r_{aroot} = 0.001$ m) as follows:

$$B_{fine} = \frac{l_{aroot}}{SRL} \quad \text{(S53)}$$

$$l_{aroot} = \frac{A_l}{2\pi r_{aroot} A_l{:}A_r} \quad \text{(S54)}$$

In all simulations in this paper $A_l{:}A_r$ = 1 unless otherwise specified.

4.2 Rhizosphere

4.2.1 Compartment depths

The effective depth at which water is assumed to exist in the rhizosphere compartments (shells) is the same as the transporting and absorbing root compartments:

$$z_i = z_{nstem+1} = z_{nstem+2} = -D(Y = 0.5) \quad n_{stem} + 2 < i \leq n_{stem} + n_{shell} + 2 \qquad \text{(S55)}$$

4.2.1 Compartment sizes

The total volume (m^3) of the characteristic rhizosphere is constant for all absorbing roots of all trees and is dependent on the total community root length ($l_{aroot,i}$) as given by Eqn S20. The volume of each rhizosphere shell is given by

$$V_{i+(n_{stem}+2)} = \begin{cases} \pi Z_{soil}(r_{out,k} - r_{aroot})^2 & k = 1 \\ \pi Z_{soil}(r_{out,k} - r_{out,k-1})^2 & 1 < k \leq n_{shell} \end{cases} \qquad \text{(S56)}$$

where $r_{out,k}$ is the outer radius of the k^{th} rhizosphere shell (m) and rooting depth is equivalent to the soil depth, Z_{soil} (m). The total volume of a given rhizosphere shell (m^3) across all absorbing roots of the j^{th} tree is

$$V_{i,j} = V_i \frac{l_{aroot,j}}{Z_{soil}} \quad (n_{stem} + 2) < i \leq (n_{stem} + n_{shell} + 2) \qquad \text{(S57)}$$

5. Numerical Solution

The following scheme closely follows that developed by Zong-Liang Yang (unpublished manuscript) and is used by the Community Land Model (Oleson et al., 2010) for numerical solution of soil water fluxes. The numerical solution uses a mass-based solution to the Richards' equation, thereby doing away with the need for an iterative (potentially computationally intensive) Newton-Raphson scheme. If mass balance is not achieved within a timestep (currently 1 hour) the timestep is halved until mass balance is achieved (Ross, 2003).

5.1 Setup

The terms and array indexing below adhere to the schematic in Fig S1.1. First we approximate the Richards' mass balance equation with a finite difference scheme. This mass balance equation is in terms of total fluxes (Q units kg s^{-1}) as opposed to fluxes on a per area basis because of the different geometries within the system. Fluxes are evaluated implicitly at the t+1st timestep (superscript denotes timestep):

$$\frac{\Delta W_i}{\Delta t} = \frac{\Delta \theta_i V_i \rho_w}{\Delta t} = -Q_{i-1}^{t+1} + Q_i^{t+1} \qquad \text{(S58)}$$

Where ΔW_i and $\Delta \theta_i = \theta_i^{t+1} - \theta_i^t$ are the change in water mass (kg) and volumetric water content (m^3 m^{-3}), respectively, for soil/plant compartment i over timestep Δt (s), and ρ_w is the density of water (kg m^{-3}). Next we linearize the water fluxes about $\partial \theta$ using a Taylor series expansion as

$$Q_i^{t+1} = Q_i^t + \frac{\partial Q_i}{\partial \theta_i}\Delta\theta_i + \frac{\partial Q_i}{\partial \theta_{i+1}}\Delta\theta_{i+1} \quad \text{(S59)}$$

$$Q_{i-1}^{t+1} = Q_{i-1}^t + \frac{\partial Q_{i-1}}{\partial \theta_{i-1}}\Delta\theta_{i-1} + \frac{\partial Q_{i-1}}{\partial \theta_i}\Delta\theta_i \quad \text{(S60)}$$

Substitution of these expressions into Eqn (S58) results in a tridiagonal set of the form

$$r_i = a_i\Delta\theta_{i-1} + b_i\Delta\theta_i + c_i\Delta\theta_{i+1} \quad \text{(S61)}$$

where

$$r_i = Q_{i-1}^t - Q_i^t \quad \text{(S62)}$$

$$a_i = -\frac{\partial Q_{i-1}}{\partial \theta_{i-1}} \quad \text{(S63)}$$

$$b_i = \frac{\partial Q_i}{\partial \theta_i} - \frac{\partial Q_{i-1}}{\partial \theta_i} - \frac{V_i\rho_w}{\Delta t} \quad \text{(S64)}$$

$$c_i = \frac{\partial Q_i}{\partial \theta_{i+1}} \quad \text{(S65)}$$

Q_{i-1}^t and Q_i^t are given by Eqn. S1 and subsequent adjoining equations by using the water potentials and water contents throughout the continuum at the current timestep. The partial derivatives of boundary fluxes with respect to adjacent compartment water contents are obtained by using the chain rule:

$$\frac{\partial Q_{i-1}}{\partial \theta_{i-1}} = \frac{\partial Q_{i-1}}{\partial \psi_{i-1}}\frac{d\psi_{i-1}}{d\theta_{i-1}} \quad \text{(S66)}$$

$$\frac{\partial Q_{i-1}}{\partial \theta_i} = \frac{\partial Q_{i-1}}{\partial \psi_i}\frac{d\psi_i}{d\theta_i} \quad \text{(S67)}$$

$$\frac{\partial Q_i}{\partial \theta_i} = \frac{\partial Q_i}{\partial \psi_i}\frac{d\psi_i}{d\theta_i} \quad \text{(S68)}$$

$$\frac{\partial Q_i}{\partial \theta_{i+1}} = \frac{\partial Q_i}{\partial \psi_{i+1}}\frac{d\psi_{i+1}}{d\theta_{i+1}} \quad \text{(S69)}$$

The derivatives of the water potential –water content relationships ($\frac{d\psi_i}{d\theta_i}$) are given for plant and soil porous media types in Eqns S34 and S36, respectively. The derivatives of the fluxes with

respect to water potential in adjacent compartments ($\frac{\partial Q_{i-1}}{\partial \psi_{i-1}}$, $\frac{\partial Q_{i-1}}{\partial \psi_i}$, $\frac{\partial Q_i}{\partial \psi_i}$, $\frac{\partial Q_i}{\partial \psi_{i+1}}$) are given by applying the product rule of differentiation to Eqn S1:

$$\frac{\partial Q_{i-1}}{\partial \psi_{i-1}} = -K_{i-1}\frac{\partial(\Delta h_{i-1})}{\partial \psi_{i-1}} - \Delta h_{i-1}\frac{\partial K_{i-1}}{\partial \psi_{i-1}} \tag{S70}$$

$$\frac{\partial Q_{i-1}}{\partial \psi_i} = -K_{i-1}\frac{\partial(\Delta h_{i-1})}{\partial \psi_i} - \Delta h_{i-1}\frac{\partial K_{i-1}}{\partial \psi_i} \tag{S71}$$

$$\frac{\partial Q_i}{\partial \psi_i} = -K_i\frac{\partial(\Delta h_i)}{\partial \psi_i} - \Delta h_i\frac{\partial K_i}{\partial \psi_i} \tag{S72}$$

$$\frac{\partial Q_i}{\partial \psi_{i+1}} = -K_i\frac{\partial(\Delta h_i)}{\partial \psi_{i+1}} - \Delta h_i\frac{\partial K_i}{\partial \psi_{i+1}} \tag{S73}$$

The terms $\frac{\partial(\Delta h_{i-1})}{\partial \psi_{i-1}}$ and $\frac{\partial(\Delta h_i)}{\partial \psi_i}$ versus $\frac{\partial(\Delta h_{i-1})}{\partial \psi_i}$ and $\frac{\partial(\Delta h_i)}{\partial \psi_{i+1}}$ in Eqns S70-S73 respectively denote the derivative of total pressure head difference across compartment boundaries with respect to the water potential in the adjacent compartment that is *closer to* versus *further from* the canopy. These are given by differentiation of Eqn S2:

$$\frac{\partial(\Delta h_{i-1})}{\partial \psi_{i-1}} = \frac{\partial(\Delta h_i)}{\partial \psi_i} = 1 \tag{S74}$$

$$\frac{\partial(\Delta h_{i-1})}{\partial \psi_i} = \frac{\partial(\Delta h_i)}{\partial \psi_{i+1}} = -1 \tag{S75}$$

The terms $\frac{\partial(K_{i-1})}{\partial \psi_{i-1}}$ and $\frac{\partial(K_i)}{\partial \psi_i}$ versus $\frac{\partial(K_{i-1})}{\partial \psi_i}$ and $\frac{\partial(K_i)}{\partial \psi_{i+1}}$ in Eqns S70-S73 respectively denote the derivative of the total boundary conductance with respect to the water potential in the adjacent compartment that is *closer to* versus *further from* the canopy. These are given by differentiation of Eqn S3:

$$\frac{\partial K_i}{\partial \psi_i} = \begin{cases} \begin{cases} 0 & \Delta h_i < 0 \\ K_{max,i}\dfrac{d(FMC_i)}{d\psi_i} & \Delta h_i \geq 0 \end{cases} & i \neq n_{stem}+2 \\ K_{max,aroot,radial}\left(\dfrac{K_i}{K_{max,aroot,radial}FLC_i}\right)^2\dfrac{d(FLC_i)}{d\psi_i} & i = n_{stem}+2 \end{cases} \tag{S76}$$

$$\frac{\partial K_i}{\partial \psi_{i+1}} = \begin{cases} \begin{cases} K_{max,i}\dfrac{d(FMC_{i+1})}{d\psi_{i+1}} & \Delta h_i < 0 \\ 0 & \Delta h_i \geq 0 \end{cases} & i \neq n_{stem}+2 \\ K_{max,aroot\leftrightarrow r_{node,1}}\left(\dfrac{K_i}{K_{max,aroot\leftrightarrow r_{node,1}}FLC_{i+1}}\right)^2\dfrac{d(FLC_{i+1})}{d\psi_{i+1}} & i = n_{stem}+2 \end{cases} \tag{S77}$$

where, as in Eqn S3, $\Delta h_i < 0$ and $\Delta h_{i-1} < 0$ indicate flow towards and away from the canopy, respectively. Equations for $\frac{\partial K_{i-1}}{\partial \psi_{i-1}}$ and $\frac{\partial K_{i-1}}{\partial \psi_i}$ are not given as they are identical to Eqns S76 and S77, respectively, after substituting $i = i - 1$.

In Eqns S76 and S77, $K_{max,i}$ is given by Eqns S14 and S19 (plant) and S25b (rhizosphere). $K_{max,aroot,radial}$ (the total resistance of absorbing roots from their surface to xylem) and $K_{max,aroot \leftrightarrow r_{node,1}}$ (the total soil resistance from the innermost rhizosphere node to absorbing root surface) are given by Eqns S19 and S25a, respectively. $\frac{d(FMC_i)}{d\psi_i}$ is given by Eqns S37 (plant compartments) and S39 (rhizosphere). The total boundary conductance, K_i, is given by Eqn S2 and adjoining equations, and the fractional loss of conductance, FMC_i, is given by Eqn 4 in the main text (plant) and Eqn S38 (rhizosphere).

5.2 Boundary conditions

For the outermost rhizosphere element ($i = n_{stem} + n_{shell} + 2$), the boundary condition is taken as zero-flow and the tridiagonal set becomes

$$r_i = Q_{i-1}^t \tag{S78}$$

$$a_i = -\frac{\partial Q_{i-1}}{\partial \theta_{i-1}} \tag{S79}$$

$$b_i = -\frac{\partial Q_{i-1}}{\partial \theta_i} - \frac{V_i \rho_w}{\Delta t} \tag{S80}$$

$$c_i = 0 \tag{S81}$$

For the leaf compartment ($i = 0$), the boundary condition at the current timestep t (Q_{top}^t; kg s^{-1}) is the leaf transpiration rate E_l (kg m^{-2} crown area s^{-1}) times tree crown area (m^2):

$$Q_{top} = E_l A_{crown} \tag{S82}$$

The tridiagonal set (Eqns S62-S65) for $i = 0$ becomes

$$r_i = Q_{top}^t - Q_i^t \tag{S83}$$

$$a_i = 0 \tag{S84}$$

$$b_i = \frac{\partial Q_i}{\partial \theta_i} - \frac{\partial Q_{top}}{\partial \theta_i} - \frac{V_i \rho_w}{\Delta t} \tag{S85}$$

$$c_i = \frac{\partial Q_i}{\partial \theta_{i+1}} \tag{S86}$$

5.3 Estimating the "tendency" term: sensitivity of Q_{top} to changes in leaf water content

An important term in S85 is the "tendency" term $\frac{\partial Q_{top}}{\partial \theta_0}$ (kg m^3 m^{-3} s^{-1}), which represents how the total transpiration rate changes as leaf water content changes. This term arises because stomatal conductance is a function of leaf water potential (Eqn 5 for FMC_{gs} in the main text), and leaf water potential is a function of leaf water content by the PV curve equations of the plant hydraulics model (Eqns S28-S30). The inclusion of this term causes a net reduction of total tree transpiration, particularly during the dry season when afternoon hydraulic limitation occurs (Fig. S3.3). We estimated this partial derivative by tracking its component partial derivatives back to the partial derivative of stomatal conductance, g_{sw} (mol m^{-2} s^{-1}), with respect to FMC_{gs} as follows. First, we expanded $\frac{\partial Q_{top}}{\partial \theta_0}$ into terms estimated from the plant hydraulics constitutive equations ($\frac{\partial FMC_{gs}}{\partial \psi_0}$ and $\frac{\partial \psi_0}{\partial \theta_0}$) and those which are specific to the host model's stomatal conductance scheme ($\frac{\partial E_l}{\partial FMC_{gs}}$ and its derivatives) as

$$\frac{\partial Q_{top}}{\partial \theta_0} = \frac{\partial Q_{top}}{\partial FMC_{gs}} \frac{\partial FMC_{gs}}{\partial \theta_0} = A_{crown} \frac{\partial E_l}{\partial FMC_{gs}} \frac{\partial FMC_{gs}}{\partial \psi_0} \frac{\partial \psi_0}{\partial \theta_0} \tag{S87}$$

where $\frac{\partial FMC_{gs}}{\partial \psi_0}$ and $\frac{\partial \psi_0}{\partial \theta_0}$ are given by Eqns S40 and S34, respectively. $\frac{\partial E_l}{\partial FMC_{gs}}$ derives from the hydraulics-modified TFS Medlyn stomatal conductance scheme as

$$\frac{\partial E_l}{\partial FMC_{gs}} = \frac{\partial E_l}{\partial g_{sw}} \frac{\partial g_{sw}}{\partial FMC_{gs}} \tag{S88}$$

where

$$\frac{\partial g_{sw}}{\partial FMC_{gs}} = g_0 + \left[\left(1 + \frac{g_1}{\sqrt{D_c}} \right) \frac{A_n}{c_a} \right] \tag{S89}$$

and where the remaining partial derivatives derive from the host (TFS) model energy balance scheme, which itself follows the scheme of the MAESTRA model (Medlyn et al., 2007), which in turn is based on the Penman-Monteith equation (see Equations A43-A48 in the Supplement to Fyllas et al. 2014). These remaining terms are given by assuming that changes in leaf temperature due to changes in stomatal conductance within a timestep's energy balance iteration are negligible with respect to the total upper boundary flux Q_{top}, which allows us to make a first-order analytical approximation for $\frac{\partial E_l}{\partial g_{sw}}$ as

$$\frac{\partial E_l}{\partial g_{sw}} = \frac{1}{\lambda_v} \frac{\partial LE}{\partial \gamma_s} \frac{\partial \gamma_s}{\partial g_V} \frac{\partial g_V}{\partial g_{sw}} \tag{S90}$$

where

$$\frac{\partial LE}{\partial \gamma_s} = -\frac{sR_n + g_H c_p \rho_a D_C}{(s+\gamma_s)^2} \quad \text{(S91)}$$

$$\frac{\partial \gamma_s}{\partial g_V} = \frac{\gamma g_H}{{g_V}^2} \quad \text{(S92)}$$

$$\frac{\partial g_V}{\partial g_{sw}} = \left[1 + \frac{g_{sV}}{g_{bV}}\right]^{-2} \frac{RT_K}{P} \quad \text{(S93)}$$

where λ_v is the latent heat of vaporization (= 2.454 x 10^6 J kg^{-1}), LE is latent energy flux (W m^{-2}), $\gamma_s = \gamma \frac{g_H}{g_V}$ is the psychrometric constant times the ratio of the total heat to total vapor conductance (Pa m K^{-1} s^{-1}), s is the slope of the saturation vapor pressure curve (Pa $^oK^{-1}$), R_n is the net radiation (W m^{-2}), c_p is the specific heat capacity of air (J kg^{-1} K^{-1}), ρ_a is the density of air (kg m^{-3}), D_C is the leaf-to-air vapor pressure deficit (Pa), g_{sV} is stomatal conductance to water vapor in velocity units (m s^{-1}), g_{bV} is the boundary layer conductance to water vapor (m s^{-1}), R is the gas constant (= 8.314 J mol^{-1} K^{-1}), T_K is air temperature (K), and P is air pressure (Pa).

5.4 Solution and mass balance checking

The tridiagonal set (Eqns S62-S65) is solved for each tree *j* using a standard numerical method for solving a tridiagonal matrix (Press et al., 1992). We wrapped this numerical solution within an outer do while loop to check for mass balance and halved the timestep Δt, solving within an inner loop the tridiagonal set and updating state variables for an appropriate number of sub-iterations, until mass balance was achieved or until a maximum number (= 5) of halving iterations had occurred. The equation for total mass balance error on a per unit time and volume basis (W_e; kg s^{-1} m^{-3}) for tree *j* over a timestep Δt is

$$W_{e,j} = \frac{1}{V_{tot,j}}\left[\frac{\Delta W_{tot,j}}{\Delta t} + \left(Q_{top,j} + \frac{\partial Q_{top,j}}{\partial \theta_{0,j}} \Delta\theta_{0,j}\right)\right] \quad \text{(S94)}$$

where $\Delta W_{tot,j}$ (kg) and $\Delta\theta_{0,j}$ (m^3 m^{-3}) are the change in total water mass (tree and rhizosphere) and leaf volumetric water content over timestep Δt and are given by

$$\Delta W_{tot,j} = W_{tot,j}^{t+1} - W_{tot,j}^{t} = \left[\sum_{i=0}^{i=n_{stem}+n_{shell}+2} \theta_{i,j}^{t+1} V_{i,j} \rho_w - \sum_{i=0}^{i=n_{stem}+n_{shell}+2} \theta_{i,j}^{t} V_{i,j} \rho_w\right] \quad \text{(S95)}$$

and

$$\Delta\theta_{0,j} = \theta_{0,j}^{t+1} - \theta_{0,j}^{t} \quad \text{(S96)}$$

We set the threshold for mass balance $|W_{err,thresh}|$ = 1.0 x 10^{-15} kg s^{-1} m^{-3}. Simulations were set to abort with an error if $|W_{err,thresh}|$ exceeded 1.0 x 10^{-1} kg s^{-1} m^{-3}. No simulations were ever aborted for the results presented in this paper.

6. Community-level soil water balance: root uptake, infiltration and drainage

6.1. Root uptake and the mean-field approximation

Different rates of root uptake across trees will lead to diverging water contents among all the individual trees' rhizospheres, but a much more complex, spatially explicit belowground hydrology model would be required to solve for fluxes among trees' rhizospheres. In order to avoid such complexity while maintaining model capability to represent rhizosphere resistance surrounding absorbing roots at the scale of millimeters, which can potentially limit root uptake and whole-plant function (Sperry et al. 1998), we assumed that soil water is kept mean-field. In other words, at the end of every timestep we averaged root water uptake in each rhizosphere shell across individuals and used the resultant value to update the water content of a single, community-level rhizosphere:

$$\Delta\theta_{k,comm} = \sum_j \Delta\theta_{i,j} \frac{l_{aroot,j}}{l_{aroot,comm}} \quad n_{stem} + 2 < i \leq n_{stem} + n_{shell} + 2 \qquad \text{(S97)}$$

Where $k = i - (n_{stem} + 2)$ indexes the single characteristic rhizosphere from 1 to n_{shell}, and it can be shown that the ratio of individual to total community absorbing root length ($\frac{l_{aroot,j}}{l_{aroot,comm}}$) represents the relative quantitative contribution of tree *j*'s root uptake in shell k.

Thus, a single, unique radial profile of soil water content is applied to all trees' rhizospheres when solving the 1D plant hydraulics equations given in the sections above. This also simplifies solving for infiltration and drainage fluxes, which are also done on a mean-field basis (see below). An alternative approach (while avoiding the complexities associated with computing horizontal water fluxes) would be to assume that each tree has its own rhizosphere which is in no way connected to adjacent trees' rhizospheres and hence, under drought, trees with large initial rates of root uptake may become rhizosphere-limited before adjacent trees with smaller initial rates of root uptake. These alternative approaches comprise, respectively, extremes on a spectrum of complete to zero horizontal mixing of soil water. Reality likely lies somewhere in between. However, we chose the former because water is not a directional resource, in contrast to light, which is a dominant reason for spatial crown segregation. In addition, the limited evidence in tropical forests suggests the balance tips in favor of spatial desegregation of individual horizontal root distributions (see Jones et al., 2011). More complex belowground hydrological models are needed to explore the impacts of such assumptions and to suggest alternative approximations for the problem of horizontal mixing of soil water.

6.2. Infiltration and Drainage

The infiltration in our model remained the same as that in TFS v.1 (Fyllas et al. 2014), following a runoff curve number (CN) method (Cronshey et al., 1986). The potential maximum retention after runoff begins, S (mm), is a function of an empirical parameter CN [0-100] that indicates a lower potential for runoff for small numbers and a higher potential for runoff for large numbers:

$$S = \frac{1000}{CN} - 10 \qquad \text{(S98)}$$

Because of the high infiltration rates often reported for tropical soils (Renck and Lehmann, 2004), we chose a relatively low value of 50 for CN. The equation for runoff rate (Q_{RO}; mm s^{-1}) over some time interval Δt (s) is

$$Q_{RO}\Delta t = \begin{cases} 0 & P \leq I_a \\ \dfrac{(P - I_a)^2}{(P - I_a) + S} & P > I_a \end{cases} \quad \text{(S99)}$$

where the initial abstraction (I_a; mm), which is the sum of all losses to infiltration before runoff begins and includes vegetation interception, evaporation and ponding, is approximated as (Cronshey et al., 1986)

$$I_a = 0.2S \quad \text{(S100)}$$

So that Eqn S99 reduces to

$$Q_{RO}\Delta t = \begin{cases} 0 & P \leq 0.2S \\ \dfrac{(P - 0.2S)^2}{P + 0.8S} & P > 0.2S \end{cases} \quad \text{(S101)}$$

We approximated vertical drainage rate (Q_{drain}; mm s^{-1}) as free drainage:

$$Q_{drain} = \frac{9.8}{10^3} k_{max.soil} FMC_{soil}\left(\psi_{soil,avg}\right) \quad \text{(S102)}$$

Where $FMC_{soil}\left(\theta_{soil,avg}\right)$ is the unsaturated hydraulic conductivity curve (Eqn S38) evaluated using the mean soil matric potential $\psi_{soil,avg}$, across all rhizosphere shells:

$$\psi_{soil,avg} = \frac{1}{\sum_{k=1}^{k=n_{shell}} V_k} \sum_{k=1}^{k=n_{shell}} \psi_k V_k \quad \text{(S103)}$$

6.3. Partitioning vertical fluxes across rhizosphere shells

Because $Q_{net} = P - Q_{RO} - Q_{drain}$ (where P is precipitation rate; mm s^{-1}) gives the net rate of water gain or loss from the total soil water pool yet soil water is tracked on a rhizosphere shell-specific basis, we had to consider how Q_{net} is partitioned across rhizosphere shells of differing water contents and matric potentials. As this is a problem of tracking mass balance across two disparate scales (mm length scale of the rhizosphere versus the larger length scale of vertical water flux), it has no analytical solution. We therefore chose the simplest algorithm that would respect the general principle that a net gain of water ($Q_{net} > 0$) should preferentially wet the driest rhizosphere shells, while a net loss of water ($Q_{net} < 0$) should preferentially drain the wettest rhizosphere shells. Thus, for $Q_{net} > 0$, we ordered the rhizosphere shells in terms of increasing water content and filled each shell (and any shell with equivalent water content) with the available water up to the next highest (in terms of water content) rhizosphere shell, and repeated this process until Q_{net} was exhausted or saturation of all rhizosphere shells was reached, in which case any remaining Q_{net} was diverted to Q_{RO}. Similarly, for $Q_{net} < 0$, we

ordered the rhizosphere shells in terms of decreasing water content and drained each shell down to the next-lowest (in terms of water content) rhizosphere shell until Q_{net} was exhausted or the residual water content of all rhizosphere shells was reached.

References

Cosby, B. J., Hornberger, G. M., Clapp, R. B., and Ginn, T. R.: A Statistical Exploration of the Relationships of Soil Moisture Characteristics to the Physical Properties of Soils, Water Resources Research, 20, 682-690, 1984.

Cronshey, R., McCuen, R. H., Miller, N., Rawls, W., Robbins, S., and Woodward, D.: Urban hydrology for small watersheds, TR-55. Conservation Engineering Division, USDA Natural Resources Conservation Service, 1986.

Fisher, R. A., Williams, M., Do Vale, R. L., Da Costa, A. L., and Meir, P.: Evidence from Amazonian forests is consistent with isohydric control of leaf water potential, Plant Cell Environ., 29, 151-165, 2006.

Gardner, W. R.: Dynamic aspects of water availability to plants, Soil Science, 89, 1960.

Jones, F. A., Erickson, D. L., Bernal, M. A., Bermingham, E., Kress, W. J., Herre, E. A., Muller-Landau, H. C., and Turner, B. L.: The Roots of Diversity: Below Ground Species Richness and Rooting Distributions in a Tropical Forest Revealed by DNA Barcodes and Inverse Modeling, Plos One, 6, 2011.

Metcalfe, D. B., Meir, P., and Williams, M.: A comparison of methods for converting rhizotron root length measurements into estimates of root mass production per unit ground area, Plant Soil, 301, 279-288, 2007.

Niklas, K. J.: Modelling below- and above-ground biomass for non-woody and woody plants, Ann Bot, 95, 315-321, 2005.

Oleson, K. W., Lawrence, D. M., Bonan, G. B., Flanner, M. G., Kluzek, E., Lawrence, P. J., Levis, S., Swenson, S. C., Thornton, P. E., and al., e.: Technical description of version 4.0 of the Community Land Model (CLM), National Center for Atmospheric Research, Boulder, CO, USA, 257 pp., 2010.

Renck, A. and Lehmann, J.: Rapid Water Flow and Transport of Inorganic and Organic Nitrogen in a Highly Aggregated Tropical Soil, Soil Science, 169, 330-341, 2004.

Ross, P. J.: Modeling soil water and solute transport - Fast, simplified numerical solutions, Agronomy Journal, 95, 1352-1361, 2003.

Savage, V. M., Bentley, L. P., Enquist, B. J., Sperry, J. S., Smith, D. D., Reich, P. B., and von Allmen, E. I.: Hydraulic trade-offs and space filling enable better predictions of vascular structure and function in plants, Proceedings of the National Academy of Sciences, 107, 22722-22727, 2010.

Siau, J. F.: Transport processes in wood, Springer Verlag, Berlin, Germany, 1984.

Sperry, J. S., Adler, F. R., Campbell, G. S., and Comstock, J. P.: Limitation of plant water use by rhizosphere and xylem conductance: results from a model, Plant, Cell & Environment, 21, 347-359, 1998.

Stewart, G. R., Gracia, C. A., Hegarty, E. E., and Specht, R. L.: Reductase Activity and Chlorophyll Content in Sun Leaves of Subtropical Australian Closed-Forest (Rainforest) and Open-Forest Communities, Oecologia, 82, 544-551, 1990.

Tomasella, J. and Hodnett, M. G.: Marked differences between van Genuchten soil water-retention parameters for temperate and tropical soils: a new water-retention pedo-transfer functions developed for tropical soils, Geoderma, 108, 155-180, 2002.

Tyree, M. T. and Hammel, H. T.: Measurement of Turgor Pressure and Water Relations of Plants by Pressure-Bomb Technique, Journal of Experimental Botany, 23, 267-&, 1972.

van Genuchten, M. T.: A closed-form equation for predicting the hydraulic conductivity of unsaturated soils, Soil science society of America journal, 44, 892-898, 1980.

Yamakura, T., Hagihara, A., Sukardjo, S., and Ogawa, H.: Aboveground biomass of tropical rain forest stands in indonesian borneo, Vegetatio, 68, 71-82, 1986.

Zeng, X.: Global Vegetation Root Distribution for Land Modeling, Journal of Hydrometeorology, 2, 525-530, 2001.